Water defect stabilizes Bi^{3+} lone-pair electronic state leading to an unusual aqueous hydration structure.

Darren M. Driscoll[b], Richard C. Shiery[c], Nicolas D'Annunzio[a], Daria Boglaienko[a], Mahalingam Balasubramanian[b]*, Tatiana G. Levitskaia[a], Carolyn I. Pearce[a]*, Niranjan Govind[a]*, David C. Cantu[c]*, John L. Fulton[a]*

[a]Pacific Northwest National Laboratory, Richland, Washington 99354, USA.

[b]Advanced Photon Source, Argonne National Laboratory, Argonne, IL 60439, USA

[c]Chemical and Materials Engineering, University of Nevada, Reno, Reno, NV 89557, USA

ABSTRACT: The aqueous hydration structure of the Bi^{3+} ion is probed using a combination of extended X-ray absorption fine structure (EXAFS) spectroscopy and density functional theory (DFT) simulations of ion-water clusters and of condensed-phase solutions. Anomalous features in the EXAFS spectra are found to be associated with a highly asymmetric first-solvent water shell. The aqueous chemistry and structure of the Bi^{3+} ion is dramatically controlled by the water stabilization of a lone-pair electronic state involving the mixed 6*s* and 6*p* orbitals. This leads to a distinct multi-modal distribution of waters in the first shell that are separated by about 0.2 Å. The lone-pair structure is stabilized by a collective response of multiple waters that are localized near the lone-pair anti-bonding site. The findings indicate that the lone-pair stereochemistry of aqueous Bi^{3+} ions play a major role in the binding of water and ligands in aqueous solutions.

1. INTRODUCTION

The chemistry of bismuth (Bi) is of importance for the production of pharmaceuticals,[1, 2] for the replacement of lead with Bi-metal alloys, and in geochemistry. In geochemistry, the critical role of Bi compounds in the aqueous hydrothermal transport and concentration of precious metals has been reported.[3] There is recent high-interest in the use of Bi-based materials for novel environmental remediation applications. As an environmentally benign element with low toxicity, bismuth compounds show exceptionally high efficiency at capturing toxic and radioactive anions.[4-6] This high affinity for multiple negatively charged contaminants is based on the electronic and structural flexibility of the Bi-based materials. The hydrolysis of aqueous Bi^{3+} causes the formation of polyatomic oxyhydroxide clusters e.g., $[Bi_6O_4(OH)_4]^{6+}$ as initial transient species. This flexible structure based on clusters can easily transform into crystalline Sillén phases containing $[Bi_2O_2]^{2+}$ sheets, with charge-balancing anions as intervening layers.[7] Thus, it is important to understand the aqueous chemistry of Bi^{3+} so that solution conditions can be tailored to control hydrolysis and form stable structures able to incorporate contaminants of concern.[8]

The electronic state of Bi^{3+} – having the simplicity of the completely filled valence electron shells as [Xe] $4f^{14}5d^{10}6s^2$– belies the complexity of its chemistry. The structure of a large number of Bi^{3+} compounds is affected by a stereochemically active lone-pair configuration.[2] This process involves mixing of Bi^{3+} 6*s* and 6*p* orbitals at non-centrosymmetric sites. In particular, the associating ligands or counterions play a role due to a strong interaction between the Bi 6*s* and the ligand 2*p* orbitals (e.g. O^{2-}) that results in high-energy anti-bonding states with a considerable degree of cation *s* character at the top of the upper valence band.[9] The Bi(III) 6*s* lone pair imparts unusual properties to solids and interfaces. In particular, the pyrochlore structure of the Bi-containing metal oxides, $Bi_2Ru_2O_{7-y}$, have received attention. The bulk metal oxide is a metallic conductor[10, 11] where the Bi(III) atom is found to be off-center from the ideal crystalline position because of lone-pair distortion. In addition, this Bi ruthenate compound has an interfacial configuration that is known in electrochemistry for its efficiency in O_2 reduction.[12] In this respect, Hamnett[12] proposed that the Bi(III) surface atom site is not strongly hydrated since the low effective symmetry of the surface site stabilizes the externally-oriented lone-pair structure. Hence the binding of water at this surface site is significantly weakened allowing O_2 to displace the outer layer of water overcoming a key limiting step in the reduction cycle. Although it might reasonably be assumed that an aqueous Bi^{3+} ion might also adopt a lone-pair active configuration such a structure has never been reported. Observation of a

stereochemically active lone pair ion would significantly alter the present understanding of aqueous Bi^{3+} chemistry

Studies of aqueous Bi^{3+} have thus far suggested a lesser role for lone-pair stereochemical effects. Often, optimized ion-water clusters are a bellwether for the ion hydration structure in the liquid phase. Ion-water cluster optimizations from electronic structure calculations (MPW1PW91)[13] have been reported for the series, $Bi^{3+}\bullet (H_2O)_n$ (n = 7,8,9) showing very symmetric structures with mean Bi-O distances of $\bar{x}_7 = 2.46$, $\bar{x}_8 = 2.49$, and $\bar{x}_9 = 2.53$ Å, respectively and very low bond disorder (typically $\sigma^2 < 0.001$ Å^2). For comparison, a stable nonaaqua-Bi^{3+} crystalline compound has been produced from trifluoromethane sulfonate, in which the single water shell is stabilized by centrosymmetric placement of the anions about the nonaaqua-Bi^{3+}. This crystalline $[Bi^{3+}(H_2O)_9](SO_3CF_3^-)_3$ has Bi-O distances of (6x) 2.448 Å and (3x) 2.577 Å (or $\bar{x}_9 = 2.49$ Å ($\sigma^2 = 0.004$ Å^2)) that are in reasonable agreement with optimized ion-water cluster results. This crystalline compound also has relatively low bond disorder.

Molecular dynamics simulations have been used to predict the condensed phase ion-water structure. A modified QM/MM approach[14] yielded a 9-fold coordination with a Bi−O distance of 2.51 Å ($\sigma^2 =$ 0.022 Å^2). More recent ab initio molecular dynamics simulations, at the PBE/GGA level of theory[15] also revealed a mono-modal peak in the Bi-O g(r) at a distance of 2.41 Å($\sigma^2 =$ 0.017 Å^2). In this case a seven-coordinate aqua ion was observed. In reviews of ion-water structures, the contributions of Bi lone pair stereochemistry on the hydration structure is deemed to be less important.[2, 16] Earlier experimental EXAFS and X-ray diffraction (XRD) measurements apparently supported these findings with Bi−O distance of 2.41 Å ($\sigma^2 =$ 0.013 Å^2).[17]

It is interesting to compare Bi^{3+} to another *f*-electron, trivalent cation, Dy^{3+}, that lies to the left of Bi in the same row of the periodic table and that would not have lone-pair stereochemical effects. The measured Dy-O distance[18] (2.38 Å) is about the same as that for Bi-O (2.41Å).[17] In contrast, the Debye-Waller factor for the Bi^{3+} ion is nearly twice as large ($\sigma^2 =$ 0.013 Å^2) as that for Dy^{3+} ($\sigma^2 =$ 0.007 Å^2), thus alluding to an unusually high degree of water disorder about the Bi^{3+} aqua ion. The first hydrolysis constant, $\log \beta_1$, typically shows a linear dependence on the ratio of charge to M-O distance, z/d.[19] Although their average M-O distances are approximately the same, their $\log \beta_1$ values are vastly different, with -7.53 for Dy^{3+} and -0.92 for Bi^{3+}.[20, 21] This is another indicator of the anomalous behavior of aqueous Bi^{3+} ions.

Here we report an extensive experimental and DFT study of the aqueous Bi^{3+} structure that is based upon an evaluation of the L_3- and L_1-edge EXAFS spectra. Contrary to the prevailing concept, the results point to a very asymmetric first-shell structure about Bi^{3+}. A detailed understanding of the unusual water ordering about Bi^{3+} is resolved using various levels of DFT theories including (i) a series of large, optimized ion-water clusters and (ii) molecular dynamics (DFT-MD) trajectories with different functionals. The results show that hybrid DFT (e.g. PBE0 rather than PBE) is essential in quantitatively capturing the lone-pair induced water hydration structure measured experimentally. The proper representation of the highly asymmetric lone-pair structure of aqueous Bi^{3+} can only be obtained from optimization of clusters having two or more water shells, while single water-shell clusters generate only symmetric structures. Finally, MD-EXAFS spectra are calculated directly from these MD trajectories for direct comparison to the experimental results using methods that have been recently been applied to study of lanthanide trivalent aqua ions[22] and other ions.[23]

The findings show that an accurate accounting of the Bi^{3+} lone-pair stereochemistry is essential to predict the unusual hydration structure. Further, a collective response in the H-bonding structure of at least three waters, as a local hydration "defect", accommodates the Bi^{3+} transition to a lone-pair configuration. These results point to a much larger role than widely believed for Bi^{3+} lone-pair stereochemistry in the cation-ligand association of aqueous Bi^{3+} complexes.

2. METHODS

2.1 Aqueous Bi^{3+} sample preparation. Trifluoromethanesulfonic acid CF_3SO_3H (Sigma-Aldrich, ReagentPlus®, ≥99%) with purity validated by titration to be in the 99.0 - 101.0 % range was obtained in sealed glass ampules and used immediately after opening. Perchloric acid $HClO_4$ (Fisher Scientific, Optima™, 70 w%) with acid content of 67 w% established by titration was used as received. The aqueous acid solutions (0.3 – 6 M) were prepared with distilled deionized water (DIW, ≥ 18 MΩ-cm). Both CF_3SO_3H and $HClO_4$ are among the strongest known acids with the respective estimated pK_a values of −15.2±2.0 and −14.7±2.0.[24] Therefore, at the tested concentrations in aqueous solutions, both acids predominantly exist as dissociated ions. Non-coordinating nature of both ClO_4^- and $CF_3SO_3^-$ anions as ligands for trivalent lanthanide ions in aqueous solutions is well-established.[25] Bismuth(III) oxide Bi_2O_3 (Sigma-Aldrich, nanopowder, 99.8% trace metals basis) was dissolved directly in the acid solutions, and pH was measured (Table 1).

2.2 Experimental measurement of extended X-ray absorption fine structure spectra. X-ray absorption fine structure measurements were performed on the L_3- and L_1-edges of aqueous-Bi solutions at 20-BM of the Advanced Photon Source. Solutions were deposited in liquid holders of specific thickness depending on the solution concentration (PEEK cell, kapton windows, sealed with epoxy) in order to provide edge-heights of about 0.5 or 0.1 at the L_3- or L_1-edges, respectively. Spectra for the highly dilute Bi^{3+} solutions were run in fluorescence mode. A Si(111) monochromator was used and the Rh-coated harmonic rejection mirror set to cut-off energy of 22.3 keV. The incident beam was detuned by approximately 15% at the center of the EXAFS scan. Energy calibration was performed through periodic measurements of a Pb foil. XAS analysis utilized the Athena and Artemis software packages.[26] The absorption edge was normalized and the extraction of the χ(k) was performed through the use of a spline function with a cutoff distance (R_{BKG}) of 1.2Å. A portion of the analysis involves convential EXAFS fitting using the Artemis software. In this case both the L_3- and L_1-edge experimental spectra were simultaneously fit using theoretical standards generated for the Bi-O scattering paths (FEFF9).[27] In this case, the fit range for the L_3-edge was $1.8 < k < 14$ Å^{-1}, while that for the L_1-edge was $1.5 < k < 12.5$ Å^{-1}. The core-hole factor, S_O^2, was set to one for this procedure.

2.3 Ab initio molecular dynamics simulations (AIMD) and analysis. All atoms in the AIMD simulation boxes were modeled with density functional theory (DFT), conducted in the PBE functional[28] using the CP2K package.[29, 30] The PBE functional has been tested for water.[31, 32] Core electrons were modeled with norm-conserving GTH pseudopotentials,[33] which

were optimized considering relativistic effects. Valence electrons were modelled with polarizable double-zeta basis sets.[34] Long range electrostatic terms were determined with a supplementary planewave basis set, using a 500 Ry cutoff.[35] Grimme's D3 corrections[36] were used to account for van der Waals interactions within a 6.0 Å radius in all simulations.

AIMD simulations were done in the canonical (NVT) ensemble at room temperature with 1 fs time steps. The aqueous condensed phase was simulated with periodic boundary conditions in cubic boxes 12.42 Å in length. A Bi^{3+} ion was placed in a 64-water box at the density of water at room temperature, resulting in a Bi concentration of ~0.8 molar. Cl- anions were added to neutralize the charge; sufficient spacing between ions ensured that no ion pair formation was observed. To resolve the solution structure of the Bi^{3+} aqua ion, we ran the NVT AIMD simulations until a stable potential was observed at about 20 ps.

The stable simulation frames were used for further analysis, which includes: (i) Bi-O radial distribution functions (RDFs) to quantify frame-averaged Bi-O pair distances, (ii) O-Bi-O angle distribution functions (ADFs), and (iii) root mean square deviations (RMSD) from ideal square, square antiprism, trigonal dodecahedron (DDH), and bicapped trigonal prism (BTP) eight-coordinate geometries[37, 38] as we recently performed with the Ln^{3+} aqua ions.[22] We calculated the RMSD between the Bi^{3+} first coordination shell in AIMD frame and all reference molecular geometries and averaged them over the AIMD trajectory to quantify which reference molecular geometry the Bi^{3+} ion favors in solution.

2.4 Extended X-ray absorption fine structure spectra from ab initio molecular dynamics. MD-XAFS has been previously described.[23] We generated the $\chi(k)$ spectra from AIMD trajectories,[39] using FEFF8.5[40] to compare with experimentally measured EXAFS. From equilibrated AIMD trajectories, we extracted 200 equi-spaced frames, and retrieved the Bi and O coordinates, to generate ensemble average spectra. An MD-EXAFS spectrum is generated for each simulation frame.[23, 39] The final spectrum is an ensemble-average one, generated from 200 AIMD simulation frames. The FEFF8.5 code was adjusted to increase the default value of total paths to include all the atom backscattering out to about 8.5 Å. Only Bi and O atoms were included in the FEFF calculations because the inclusion of H atoms results in a too large number of scattering paths that fail to converge.

2.5 DFT optimizations and AIMD of Bi^{3+}–water clusters calculations. Cluster optimizations and AIMD[41] at room temperature (~0.25 fs) were generated using a Bi^{3+}–centered cluster with 40 water molecules using NWChem[42, 43]. The Bi center was represented with the relativistic def2-TZVPP effective core potential/basis set and the O and H atoms were represented with the 6-31G* basis set.[44, 45] The PBE0 exchange-correlation functional[46] was used for all calculations that also included the Grimme dispersion correction.[47] Longer range solvation effects beyond the explicit water cluster about the Bi^{3+} ion were treated with the COSMO implicit solvation model.[48] Spin-orbit effects were not included during the optimizations for the large number of configurations and for the dynamic calculations because of the high computational cost. However, we performed spin-orbit calculations on a single configuration and found a 6p splitting of ~2.1 eV. This level of spin-orbit effects is significant and points to the opportunity for even higher structural accuracy through inclusion of spin-orbit effects.

3. RESULTS AND DISCUSSION

3.1 EXAFS results predict a bimodal structure in the Bi^{3+} first shell. The EXAFS k^3-weighted $\chi(k)$ plots for 0.1 m Bi^{3+} at pH 0.0 are shown in Figure 1a. Spectra that were acquired at both the Bi L_3- and L_1-edges are shown. Notable for this aqueous cation are the anomalous decreases in the amplitudes or "beating" of the oscillations in the region around k = 6-8 $Å^{-1}$ as indicated by the arrows in Figure 1a. The fact that the same feature is observed in both the L_3- and L_1-edge spectra ($2p_{3/2}$ versus $2s$ initial states) can reasonably exclude common EXAFS artifacts in the $\chi(k)$ spectra such as multi-electron excitations and monochromator or beamline artifacts.

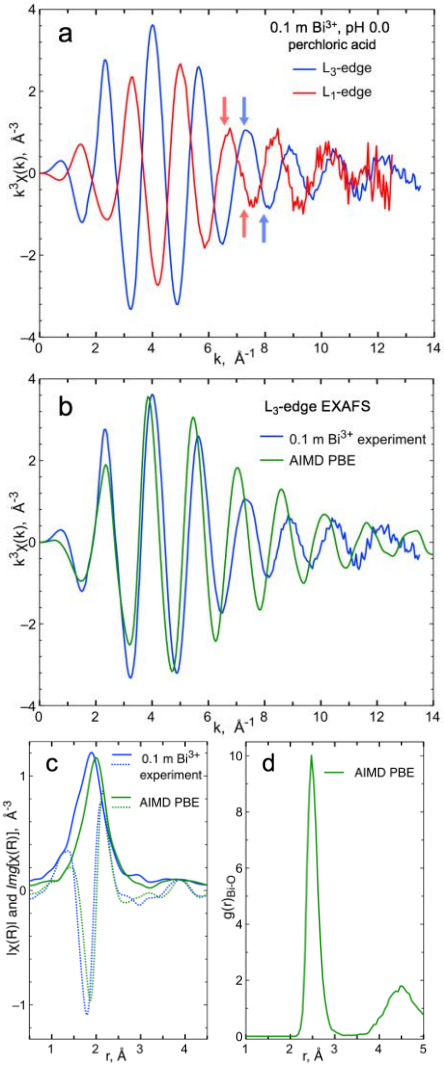

Figure 1. Comparison of experimental and theoretical EXAFS spectra. (a) the k^3-weighted $\chi(k)$ plots at both the L_3- and L_1-edges for 0.1 m Bi^{3+} in pH 0.0 perchloric acid solution. (b) comparison of the experimental L_3-edge spectrum with that for the MD-EXAFS spectrum generated from AIMD PBE trajectory. (c) the resulting k^2-weighted Fourier-transformed R plots and (d) the Bi-O pair distribution function from the AIMD PBE/Condensed Phase trajectory.

This type of anomalous amplitude decay is not observed for the divalent first-row transition metals ions[49] (with the exception of Cu^{2+} having Jahn-Teller distortion) nor for any of the

trivalent aqueous lanthanide ions[18] that lie to the left of Bi^{3+} in the same row of the periodic table, all of which show an continuous amplitude decay function. The EXAFS contributions from close-by shells with similar backscattering neighbors (e.g., oxygen), may exhibit a beat (evidenced by a "beating" pattern in the $\chi(k)$ located at k_{beat}) due to interference from individual oscillatory, $\sin 2kR$, EXAFS contributions. In the simplest case of two close-by shells, the value of k_{beat} in $\chi(k)$ will follow the relation as $R_1 - R_2 = \pi/2k_{beat}$, where R_1 and R_2 are the correlation distances of the two close-by shells with respect to the probed central absorber (bismuth). The EXAFS shown in Figure 1 shows a beat at 7 $Å^{-1}$suggesting there are at least two distinct Bi-O correlations that are separated by ~ 0.22 Å.

To further illustrate this point, Figure 1b compares the experimental L_3-edge spectrum with the spectrum generated using MD-EXAFS from the condensed phase AIMD trajectory at the PBE level of theory (Section 2.3). Since the EXAFS theory (FEFF9) is exact for a given set of atom positions, the MD-EXAFS spectrum generated from an ensemble average provides the true EXAFS spectrum corresponding to the structure of the simulation. Notable in Figure 1b, the AIMD simulation (PBE/Condensed Phase) replicates the initial and final part of the amplitude envelop over the full *k* region but not in the intermediate region of the beating. The Bi-O g(r) in Figure 1d shows a single Gaussian-like distribution centered at about 2.49 Å that would not lead to beating pattern in $\chi(k)$. The Bi-O first-shell distance in AIMD is slightly longer than the experimental value leading to a mismatch in the frequency of the oscillations in $\chi(k)$ at high *k* (2.49 vs 2.41 Å, respectively).

3.2 Exploring the presence of Bi^{3+} hydrolysis and ion pairing species. A plausible explanation for distance differentiation of the first shell waters would be the presence of a hydroxylated ion for which the Bi-O distance of the hydroxyl would be approximately 0.2 Å shorter than that of the water. For this reason, a condensed phase AIMD trajectory at the PBE level of theory (Section 2.3) of $Bi^{3+}(OH^-)\bullet(H_2O)_n$ was completed. The simulation predicts a seven-coordinate ion that includes one hydroxyl and six coordinated water molecules. The predicted AIMD structure is quite similar to the simulated structure of Marcos et al.[15] for the related monohydroxide species, $Bi^{3+}(OH^-)\bullet(H_2O)_5$. We then used the AIMD (PBE CN=7, OH=1) trajectory to calculate the MD-EXAFS spectrum and the Bi-O g(r) whose results are shown in Figure S1 and S2. Briefly, the "beating" signal in $\chi(k)$ is observed at too low of k = 5.5 $Å^{-1}$ and the amplitude of the oscillations were not reproduced at low k. For these reasons, a $Bi^{3+}(OH^-)\bullet(H_2O)_7$ species does not reproduce the experimentally observed Bi^{3+} $\chi(k)$ spectra at pH ≤ 0.0.

We also explored the reported equilibrium between free Bi^{3+} and the first hydrolysis species that has been given by various authors although there is some uncertainty about the exact pH position of this transition.[19, 50, 51] For this reason XAFS experiments were conducted at very low pH (-0.7) and low Bi^{3+} concentration (100-times lower) as shown in Table 1 in order to positively exclude the possibility of hydrolysis products. Figures S3 and S4 show that the EXAFS and XANES spectra for solutions having pH values ≤ 0.0 and a range of concentrations from 0.1 to 0.001 m Bi^{3+}. All of these spectra are identical and hence there are no measurable quantities of hydrolysis products. Furthermore, the XAFS spectra show no evidence Bi^{3+} forming contact-ion pairs with the anion. In this case the backscattering from Cl would be detectable in the EXAFS spectra from a contact-ion pair of the ClO_4^- anion with Bi^{3+}. Additionally, there were no differences in the XANES features that could be ascribe to these species. The XAFS spectra for solutions prepared from HCF_3SO_3 were identical to those prepared from $HClO_4$ (See Figures S3 and S4). In contrast when the pH values are raised to ≥ 0.3, a moderate amount of hydrolysis products was detected with extensive polymer formation (Figure S4).

Table 1. Sample concentrations for EXAFS measurements for Bi^{3+} solutions derived from perchloric and trifluoromethanesulfonic acid.

Concentrations, m			
Bi^{3+}	pH[a]	$HClO_4$	HCF_3SO_3
0.1	<-1.0	- -	6.2
0.1, 0.01, 0.001	-0.8	- -	3.5
0.1, 0.05	-0.8	3.4	- -
0.1	0.25	- -	1.0
0.1, 0.05	0.0	1.0	- -
0.1[b]	0.3	0.5	- -

[a]Nominal pH. [b]Hydrolysis and polymerization of Bi^{3+} was observed.

3.3 $Bi^{3+}\bullet(H_2O)_{7,8}$ DFT cluster optimizations. Figure 2 summarizes optimizations for several different ion-water clusters for which the first solvent shell contains 7 or 8 water molecules. The first column of structures are optimizations for cluster that contain only the first shell of waters about the cations. The second column is for clusters that have a total of 40 water, sufficient to completely populate the second shell of water about the ion. When only a single shell of water is included, the optimizations produce structures that have regular symmetries, either trigonal-square antiprism or square antiprism for the 7- and 8-coordinate systems, respectively. For both of these clusters, the average ion-water distance is quite uniform and similar to the values reported by Marcos.[13] Optimizations using hybrid DFT (PBE0) return the same symmetries but for which the average Bi-O bond distance is decreased by about 0.02 Å. The bond disorder is slightly higher for the PBE0 representation. Significant differences between PBE and PBE0 have also been reported for crystalline bismuth vanadate where the monoclinic structure can only be successfully predicted using the hybrid functional[52]

Optimizing clusters having a full second shell of water (40 H_2O total) leads to completely different ion-water structures as shown in the second column of Figure 2. The structures that have 7 or 8 waters in the first shell and that have extended water shells, have symmetries akin to a trigonal-dodecahedral (for CN 8) with one very short water, 4 or 5 equatorial waters and then two more distant waters on the axis opposite the short water bond near the lone-pair position. Figure 2 lists the Bi-O bond distances of the first-shell waters. The single, short ion-water bond is about 0.13 and 0.2 Å shorter than the equatorial waters for the 7- and 8-coordinate systems, respectively. This is an unusual and unique result for water about a mono-atomic ion. These results in Figure 2 illustrate that the transition to a lone-pair configurations requires two or more water shells.

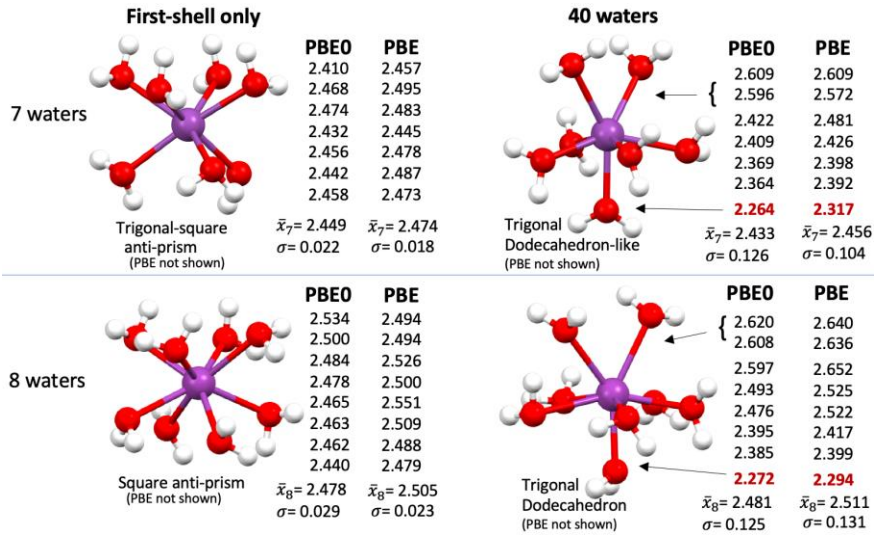

Figure 2. DFT PBE and PBE0 cluster optimizations for various configurations with the tabulated values of the Bi-O distances (Å). The set in the left column shows optimizations for systems that only contain water in the first shell. The set in the right column are results for optimizations that have a total of 40 water molecules plus the central Bi^{3+} ion. Only the first-shell waters are shown in all cases.

3.4 Evaluating symmetry from EXAFS fitting. For the 8-coordinate Bi^{3+} structures in Figure 2, two different symmetries are represented, one with equivalent Bi-O distance having square anti-prism symmetry (LHS), the other with distorted Bi-O distances having trigonal dodecahedral (t-DDH) symmetry (RHS). The classical method of fitting experimental $\chi(k)$ spectra using theoretical standards generated from (FEFF9) was used to evaluate the most probable symmetry. Table 2 reports results of simultaneously fitting both L_3- and L_1-edge spectra using theoretical standards (spectra with fits are shown in Figures S5 and S6). The fitting of the trigonal dodecahedral model (Figure 2, RHS, bottom) provides a significantly better goodness-of-fit value than the square anti-prism model (one-shell). As shown in Table 2 the fitted Bi-O distances are also in good agreement with those for the optimized PBE0 cluster. It is important to note that fitting to this t-DDH model is not a unique solution. Two- and three-shell models with other symmetries would return similar qualities of fit. What is important is that the "beating" pattern in the experimental $\chi(k)$ plots cannot be captured with a single-shell model.

The presence of the beat causes the single shell fit to exhibit lower amplitude and slight phase mismatch at high-k. Much improved reproduction of the beat, the amplitude and phase of the high-k oscillations requires the inclusion of split shells and is illustrated in the representative multi-shell fit that uses input from a cluster taken from the PBE0 cluster optimization (See Figures S5 and S6). While the need to include split Bi-O coordination is verified, the exact symmetry and CN cannot be ascertained from these fits alone.

Table 2. First-shell Bi^{3+} structure parameters derived from simultaneously fitting L_3- and L_1-edge experimental spectra using theoretical standards (FEFF9). The chosen models are based upon the trigonal dodecahedron (t-DDH) and square anti-prism (SAP) symmetries shown in Figure 2.

Model				
t-DDH	CN	R, Å	σ^2, Å^2	R, Å PBE0
$\mathcal{R}$=0.019[a]	1[b]	2.21(05)	0.011(007)	2.27
	5	2.39(01)	0.008(002)	2.47
	2	2.56(02)	0.007(003)	2.61
SAP				
$\mathcal{R}$=0.029	8.3 (0.6)	2.41(01)	0.017(001)	2.48

For 0.1 m Bi^{3+}, pH 0.0

[a]R-factor goodness of fit. [b]**Coordination numbers constrained to the defined symmetry.** Plots showing the experimental and fitted spectra are given in the Supporting Information

3.5 Water defect and the Bi^{3+} lone-pair configuration. A water defect enables the transition to the lone-pair electronic configuration of the Bi^{3+} aqua ion. The basis for this conclusion is vividly illustrated in the schematics of Figure 2. The optimized structures for Bi^{3+} with only a single water shell have nearly pure square anti-prism symmetry wherein all Bi-O distances in the first shell are nearly identical imposing a centro-symmetric ordering of the waters. The inclusion of the second shell (total of 40 waters) induces a complete rearrangement to a trigonal dodecahedral symmetry wherein one of the Bi-O bonds is anomalously short. The off-centrosymmetric distortion created by these extra waters allows the interaction with the Bi 6*s* and 6*p* states, for which the Bi lone pair is asymmetrically distributed and becomes stereochemically active.[53]

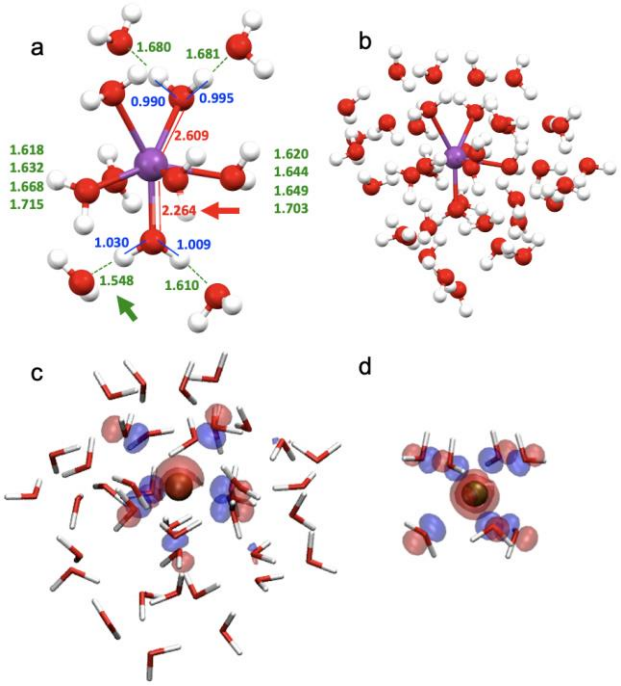

Figure 3. Further details of the water structure in Figure 2 for PBE0-optimized, 40 water cluster having 7 waters in the first shell. (a) The water bonding structure between the first and second shell shows only four selected 2nd-shell waters. The reported bond distances include ion-water (red), O-H bond (blue) and O--H hydrogen bond to second shell water (green). (b) Parent cluster. (c) Molecular orbital representations of highest-valence bonding orbitals for structure in (a). (d) The molecular orbital representations of highest-valence bonding orbitals for symmetric, first-shell water structure shown in Fig 2. In (c) and (d) red (positive) and blue (negative) isosurfaces (0.065 au).

Figure 3 more clearly illustrates the special anatomy of the Bi^{3+}-water interaction. This is an expanded view of the structure shown in Figure 2, for the cluster containing 7 waters in the first shell and 40 total waters in the cluster from the PBE0 optimization. As shown in Figure 3a, the strong distortion of first-to-second shell water H-bond only occurs in the region of the single short water and not for the equatorial nor the two apical waters. The water structure at this site is altered in two important ways, (i) the O-H bond of this water is elongated about 0.03 Å and (ii) the O--H hydrogen bonding distance to the second shell water is shortened by about 0.15Å. This anomalous first-shell water molecule is interacting with the electropositive region of the Bi^{3+}, which would be on the opposite side of the ion that contains the mixed $6s/6p$ orbitals of the lone pair. Figure 3c shows a molecular orbital representation of the bonding orbitals for the asymmetric structure in Fig 3a while orbital structure for the symmetric, single-shell water structure (Figure 2) is shown in Fig. 3d. From this comparison it is seen that two shells of water are required to induce a Bi^{3+} lone-pair configuration.

This local region in both the first- and second-solvation sphere is described as a water "defect" because the local water structure is significantly different than the bulk and that the defect involves three or more water molecules including (i) the single "bonding" water on the opposite side of the Bi^{3+} $6s$ and $6p$ lone pair, (ii) the distorted H-bonds to two waters in the second shell, (iii) and likely further propagation of the bonding to third and higher shells. The transition to the lone pair state does not occur for clusters containing a single water shell but rather requires a networking interaction of water molecules from the second water shell.

The morphology of this defect is similar to that for proton solvation as Eigen or Zundel forms in water[54] involving shortening of the H bond distance and displacement of the proton from the parent water. The propagation of the defect to higher shells also has a common basis. The short H-bond distance is similar to that found for aquated hydronium or for hydronium-Cl^- interaction.[55, 56] It is also reminiscent of the zwitterion-like water structure about the single polyatomic anion, iodate.[57]

Of significance is that this water-defect structural response will have strong effects on modes of first-shell ligand binding as well as the kinetics of water and ligand exchange. This is a unique example of a water defect influencing the water symmetry about an ion in water.

As a further note, at the lowest pH values, where the concentrations of $CF_3SO_3^-$ or $HClO_4^-$ are above 3 m, there are no first-shell interactions or contact-ion pairs with these anions as evidenced by their identical EXAFS spectra that is sensitive to the first-shell structure. However, at these high concentrations the presence of the anions in the second solvent shell is expected due to their lower solvent-to-solute molar ratios (18, e.g. 55m/3m). While the solvent response of the first- and second-water shell plays an important role in the stabilization of the lone-pair structure, these anions apparently play complementary/equivalent role in the water stabilization of the lone pair state. Both $CF_3SO_3^-$ and $HClO_4^-$ are considered to be the least interacting of known anions, but it is expected that nearly all other types of anions, including halides, likely play significant roles in the first-shell binding.

3.6 Comparing structures from AIMD trajectories. Figure 4 shows the Bi-O g(r) curves for (i) the condensed phase AIMD simulation at the PBE level of theory (Section 2.3) and (ii) 40-water cluster AIMD simulation at the PBE0 level of theory with implicit solvation (Section 2.5). Most significantly, a mono-modal distribution of Bi-O bond lengths is observed for the PBE/Condensed Phase simulation, while a multi-modal Bi-O distribution is observed for the PBE0/COSMO simulations. For the PBE0 clusters with CN = 7 and 8, there appears to be short (-0.15 Å) and long (+0.2 Å) side features as shoulders about the main g(r) peak in agreement with the cluster optimizations. As shown in Figure 4b, surprisingly, both 8-coordinate simulations show similar angle distributions. Closer analysis of the geometry of the Bi^{3+} first solvation sphere reveals that it does not strongly favor a single geometry but is in equilibrium between the DDH and SAP 8-coordinate shapes. The RMSD values (see SI) of the PBE/Condensed Phase and PBE0/COSMO simulations to the DDH, SAP geometries are 0.35+/-0.08Å, 0.38+/-0.09Å and 0.30+0.06Å, 0.41+/-0.07Å respectively: both simulations slightly favor the dodecahedral geometry, more so for the PBE0/COSMO case.

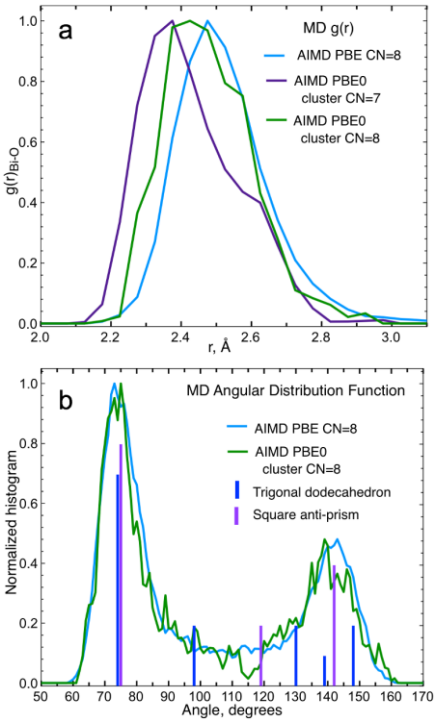

Figure 4. Bi-O pair distribution functions (a) from the AIMD trajectories for eight-coordinate PBE/Condensed Phase trajectory (blue), seven-coordinate PBE0/40waters/COSMO trajectory (purple), eight-coordinate PBE0/40waters/COSMO trajectory (green), The three plots have been normalized for comparison. The lower panel (b), shows the angular distributions functions for the eight-coordinate trajectories and the angular positions of reference standards for trigonal dodecahedron and square antiprism.

The two Bi^{3+} ion trajectories showing the multi-modal Bi-O bond length distributions were used to generate MD-EXAFS spectra.[23] Figure 5 shows that the MD-EXAFS spectra generated from the PBE0/40waters/COSMO trajectory better replicates the experimentally measured "beating" pattern than the MD-EXAFS spectra from PBE/Condensed Phase simulations (see Figure 1b). Therefore, we conclude that the aqueous Bi^{3+} ion has a lone-pair configuration structure with a multi-modal Bi-O bond length distribution. In Figure 5, the Bi^{3+} aqua ion with CN = 8, which favors the dodecaheral geometry, shows somewhat better agreement with the experimentally measured EXAFS spectrum than the CN = 7 trajectory.

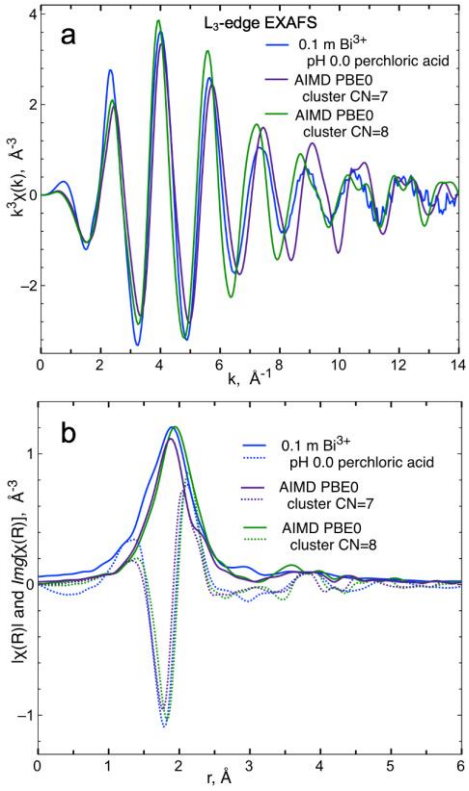

Figure 5. Comparison of experimental EXAFS and theoretical MD-EXAFS spectra. (a) the k^3-weighted $\chi(k)$ plots at L_3-edge for 0.1 m Bi^{3+} in pH 0.0 perchloric acid solution compared to the seven-coordinate PBE0/40waters/COSMO trajectory (purple) and the eight-coordinate PBE0/40waters/COSMO trajectory (green). (b) the resulting set of k^2-weighted Fourier-transformed *R* plots.

It is important to understand the limitations of the structures generated from the MD trajectories. For a trivalent cation the water exchange rates from first-to-second shell are for the most part well beyond the timescales of what is practically reasonable for DFT-MD. Free-energy calculations and thereby equilibrium distributions for different coordination numbers are beyond the scope of this paper. It is possible that the experimental system could represent an equilibrium between species with two different coordination numbers. While the results tend to suggest a single coordination number structure as the optimum, it is not possible to completely exclude the possibility of an equilibrium between two coordination number or different symmetries.

4. CONCLUSIONS

The water ordering around the Bi^{3+} ion is dominated by the lone-pair electronic state of Bi that creates an unusual hydration structure. A non-uniformity or defect in the water solvation shells stabilizes the stereochemically active Bi^{3+} lone-pair electronic configuration over that of the centro-symmetric state. While the overall width of the ion-water distribution is quite broad suggesting a high degree of disorder, quite the opposite appears to be true in that the hydrating water is well ordered about a discrete set of distances within the first coordination sphere.

The DFT-MD simulations and the hybrid DFT methods provide critical insights into these structures that can be compared directly to the experimental EXAFS spectra. The

challenge is to experimentally resolve these structures since most scattering methods used to measure atom-atom bond distances are limited by their finite spatial resolution. EXAFS is especially good in this regard, achieving a spatial resolution of about 0.12 Å in these measurements thus aiding in the understand of the structure.

Water shows a complex structure about Bi^{3+} and the expectation is that interacting anions (e.g. as contact ion pairs) or complexing ligands will also be dominated by the lone-pair chemistry. It is possible that the methodology described here will be useful for other cations such as Pb^{2+} and Sb^{3+} that also have stereochemically active lone-pair states and whose aqueous structures are presently poorly understood.

ASSOCIATED CONTENT

Supporting Information

The Supporting Information is available free of charge on the ACS Publications website.
Additional EXAFS, MD-EXAFS, XANES and g(r) data for the Bi^{3+} hydrolysis species and various Bi^{3+} concentrations. EXAFS plots for aqueous Bi^{3+} fitting of ideal square-antiprism and trigonal dodecahedral symmetry models. AIMD results for potential energy vs time from the trajectories. O-Bi-O angular distribution functions. Schematics and xyz coordinates for various 8-water symmetries. The xyz coordinates for the optimized PBE0 structure in Figure 2. RMSD with respect to ideal geometries from AIMD. xyz coordinates (Å) of the PBE AIMD starting frame. Raw XAFS experimental data will be made available upon reasonable request to the corresponding author (JF) (Word document)

AUTHOR INFORMATION

Corresponding Authors

John L. Fulton − Physical Sciences Division, Pacific Northwest National Laboratory, Richland, Washington 99352, United States; orcid.org/0000-0001-9361-9803; Email: john.fulton@pnnl.gov
David C. Cantu − Chemical and Materials Engineering, University of Nevada, Reno, Reno, Nevada 89557, United States; orcid.org/0000-0001-9584-5062;Email: dcantu@unr.edu
Niranjan Govind − *Physical Sciences Division, Pacific Northwest National Laboratory, Richland, Washington 99352*, United States; orcid.org/0000-0003-3625-366X; Email: niri.govind@pnnl.gov
Mahalingam Balasubramanian − *Advanced Photon Source, Argonne National Laboratory, Argonne, IL 60439, USA;* orcid.org/0000-0002-3988-3125;
Carolyn I. Pearce − *Pacific Northwest National Laboratory, Richland, Washington 99354, United States*; orcid.org/ 0000-0003-3098-1615; Email: carolyn.pearce@pnnl.gov

Author

Tatiana G. Levitskaia − *Nuclear Chemistry and Engineering Group, Pacific Northwest National Laboratory (PNNL), Richland, Washington 99352, United States*; Email: tatiana.levitskaia@pnnl.gov

Daria Boglaienko − *Nuclear Chemistry and Engineering Group, Pacific Northwest National Laboratory (PNNL), Richland, Washington 99352*, United States
Nicolas D'Annunzio − *Nuclear Chemistry and Engineering Group, Pacific Northwest National Laboratory (PNNL), Richland*, Washington 99352, United States
Darren M. Driscoll − *Joint Center for Energy Storage Research, Lemont, Illinois 60439, United States; Advanced Photon Source, Argonne National Laboratory, Lemont, Illinois 60439, United States*; orcid.org/0000-0001-8859-8016
Richard C. Shiery − *Chemical and Materials Engineering, University of Nevada, Reno, Reno, Nevada 89557, United States*

Author Contributions

The manuscript was written through contributions of all authors. All authors have given approval to the final version of the manuscript.

Notes

The authors declare no competing financial interest.

ACKNOWLEDGMENT

R.C.S. and D.C.C. acknowledge the donors of the American Chemical Society Petroleum Research Fund for partial support of this research, as well as the Vice President for Research and Innovation, and the College of Engineering, of the University of Nevada, Reno. C.I.P and T.G.L. acknowledge support from the Deep Vadose Zone − Applied Field Research Initiative at Pacific Northwest National Laboratory (PNNL). Work by N.G. was supported under project 72685, and J.L.F. under project 16248, funded by the U.S. Department of Energy (DOE), Office of Science, Office of Basic Energy Sciences, Division of Chemical Sciences, Geosciences, and Biosciences. Work by M.B. and D.M.D. was funded by DOE Office of Science by Argonne National Laboratory (ANL) under Contract No. DE-AC02-06CH11357. This research used resources of the Advanced Photon Source, the U.S. Department of Energy (DOE) Office of Science User Facility operated for the DOE Office of Science by Argonne National Laboratory under Contract No. DE-AC02-06CH11357. Calculations were performed in Pronghorn, the High-Performance Computing cluster of the University of Nevada, Reno, as well as in PNNL Research Computing clusters. This research also benefited from computational resources provided by EMSL, a DOE Office of Science User Facility sponsored by the Office of Biological and Environmental Research and located at PNNL. PNNL is operated by Battelle Memorial Institute for the United States Department of Energy under DOE Contract Number DE-AC05-76RL01830. This research also used resources of the National Energy Research Scientific Computing Center (NERSC), a DOE Office of Science User Facility operated under Contract DE-AC02-05CH11231.

REFERENCES

1. Weber, M.; Schlesinger, M.; Walther, M.; Zahn, D.; Schalley, C. A.; Mehring, M., Investigations on the growth of bismuth oxido clusters and the nucleation to give metastable bismuth oxide modifications. *Zeitschrift Fur Kristallographie-Crystalline Materials* **2017,** *232* (1-3), 185-207.
2. Sadler, P. J.; Li, H. Y.; Sun, H. Z., Coordination chemistry of metals in medicine:

target sites for bismuth. *Coordination Chemistry Reviews* **1999,** *185-6*, 689-709.
3. Tooth, B.; Ciobanu, C. L.; Green, L.; O'Neill, B.; Brugger, J., Bi-melt formation and gold scavenging from hydrothermal fluids: An experimental study. *Geochimica Et Cosmochimica Acta* **2011,** *75* (19), 5423-5443.
4. Ranjan, M.; Singh, P. K.; Srivastav, A. L., A review of bismuth-based sorptive materials for the removal of major contaminants from drinking water. *Environmental Science and Pollution Research* **2020,** *27* (15), 17492-17504.
5. Pearce, C. I.; Cordova, E. A.; Garcia, W. L.; Saslow, S. A.; Cantrell, K. J.; Morad, J. W.; Qafoku, O.; Matyas, J.; Plymale, A. E.; Chatterjee, S.; Kang, J.; Colon, F. C.; Levitskaia, T. G.; Rigali, M. J.; Szecsody, J. E.; Heald, S. M.; Balasubramanian, M.; Wang, S.; Sun, D. T.; Queen, W. L.; Bontchev, R.; Moore, R. C.; Freedman, V. L., Evaluation of materials for iodine and technetium immobilization through sorption and redox-driven processes. *Science of the Total Environment* **2020,** *716*.
6. Lawter, A. R.; Pearce, C. I.; Cordova, E. A.; Cantrell, K. J.; Bowden, M. E.; Lahiri, N.; Qafoku, O.; Resch, C. T.; Colon, F. C.; Boglaienko, D.; Garayburu-Caruso, V. A.; D'Annunzio, N.; Balasubramanian, M.; Saslow, S. A.; Levitskaia, T. G.; Qafoku, N.; Freedman, V. L., Mechanisms of interaction between layered bismuth materials and contaminants in sediments for subsurface remediation. *ACS Earth and Space Chemistry* **2021 submitted**.
7. Sillen, L. G., The oxyhalogenide family. *Naturwissenschaften* **1942,** *30*, 318-324.
8. Levitskaia, T. G. Q., N. P.; Bowden, M. E.; Pearce, C. I.; Asmussen, R. M.; Buck, E. C.; Freedman, V. L., A review of bismuth-based materials for remediation of contaminated sites. *ACS Earth and Space Chem.* **2021 In revision**.
9. Walsh, A.; Payne, D. J.; Egdell, R. G.; Watson, G. W., Stereochemistry of post-transition metal oxides: revision of the classical lone pair model. *Chemical Society Reviews* **2011,** *40* (9), 4455-4463.
10. Laurita, G.; Puggioni, D.; Hickox-Young, D.; Rondinelli, J. M.; Gaultois, M. W.; Page, K.; Lamontagne, L. K.; Seshadri, R., Uncorrelated Bi off-centering and the insulator-to-metal transition in ruthenium A(2)Ru(2)O(7) pyrochlores. *Physical Review Materials* **2019,** *3* (9).
11. Converse, E. S.; Li, J.; Mullins, A. C.; LaBarre, P. G.; Ramirez, A. P.; Subramanian, M. A., Influence of Alkaline-Earth-Metal Substitutions on the Bismuth Ruthenate Structure: Bi(2-x)A ' xRu2O6O '(1-y) (A ' = Mg, Ca, Sr). *Inorganic Chemistry* **2020,** *59* (19), 14141-14151.
12. Egdell, R. G.; Goodenough, J. B.; Hamnett, A.; Naish, C. C., ELECTROCHEMISTRY OF RUTHENATES .1. OXYGEN REDUCTION ON PYROCHLORE RUTHENATES. *Journal of the Chemical Society-Faraday Transactions I* **1983,** *79*, 893-912.
13. Ayala, R.; Martinez, J. M.; Pappalardo, R. R.; Marcos, E. S., Quantum-Mechanical Study on the Aquaions and Hydrolyzed Species of Po(IV), Te(IV), and Bi(III) in Water. *Journal of Physical Chemistry B* **2012,** *116* (51), 14903-14914.
14. Khan, A.; Weiss, A. K. H.; Uddin, R.; Randolf, B. R.; Rode, B. M.; Hofer, T. S., Ab Initio Quantum Mechanical Charge Field Molecular Dynamics Simulation (QMCF-MD) of Bi3+ in Water. *Journal of Physical Chemistry A* **2012,** *116* (30), 8008-8014.
15. Ayala, R.; Martinez, J. M.; Pappalardo, R. R.; Refson, K.; Marcos, E. S., Effect of Basicity on the Hydrolysis of the Bi(III) Aqua Ion in Solution: An Ab Initio Molecular Dynamics Study. *Journal of Physical Chemistry A* **2018,** *122* (7), 1905-1915.
16. Persson, I., Hydrated metal ions in aqueous solution: How regular are their structures? *Pure and Applied Chemistry* **2010,** *82* (10), 1901-1917.
17. Naslund, J.; Persson, I.; Sandstrom, M., Solvation of the bismuth(III) ion by water, dimethyl sulfoxide, N,N '-dimethylpropyleneurea, and N,N-dimethylthioformamide. An EXAFS, large-angle X-ray scattering, and crystallographic structural study. *Inorganic Chemistry* **2000,** *39* (18), 4012-4021.
18. Persson, I.; D'Angelo, P.; De Panfilis, S.; Sandstrom, M.; Eriksson, L., Hydration of lanthanoid(III) ions in aqueous solution and crystalline hydrates studied by EXAFS spectroscopy and crystallography: The myth of

the "gadolinium break". *Chemistry-a European Journal* **2008,** *14* (10), 3056-3066.
19. Baes, C. F.; Mesmer, R. S., *The Hydrolysis of Cations*. John Wiley and Sons: New York, 1976.
20. Brown, P. L.; Ekberg, C., *Hydrolysis of Metal Ions*. Wiley-VCH Verlag GmbH & Co. KGaA: Boschstr. 12, 69469 Weinheim, Germany, 2016.
21. Shiery, R. C.; Cooper, K. A.; Cantu, D. C., Computational Prediction of All Lanthanide Aqua Ion Acidity Constants. *Inorganic Chemistry* **2021,** *60* (14), 10257-10266.
22. Shiery, R. C.; Fulton, J. L.; Balasubramanian, M.; Nguyen, M. T.; Lu, J. B.; Li, J.; Rousseau, R.; Glezakou, V. A.; Cantu, D. C., Coordination Sphere of Lanthanide Aqua Ions Resolved with Ab Initio Molecular Dynamics and X-ray Absorption Spectroscopy. *Inorg. Chem.* **2021,** *60* (5), 3117-3130.
23. Schenter, G. K.; Fulton, J. L., Molecular Dynamics Simulations and XAFS (MD-XAFS). In *XAFS Techniques for Catalysts, Nanomaterials, and Surfaces*, Iwasawa, Y.; Asakura, K.; Tada, M., Eds. Springer International Publishing: Cham, 2017; pp 251-270.
24. Trummal, A.; Lipping, L.; Kaljurand, I.; Koppel, I. A.; Leito, I., Acidity of Strong Acids in Water and Dimethyl Sulfoxide. *Journal of Physical Chemistry A* **2016,** *120* (20), 3663-3669.
25. Silber, H. B.; Pezzica, A., METAL-ION ASSOCIATION IN ALCOHOL SOLUTIONS .8. LANTHANIDE AND ALKALINE-EARTH PERCHLORATES IN AQUEOUS METHANOL. *Journal of Inorganic & Nuclear Chemistry* **1976,** *38* (11), 2053-2057.
26. Ravel, B.; Newville, M., ATHENA, ARTEMIS, HEPHAESTUS: data analysis for X-ray absorption spectroscopy using IFEFFIT. *Journal of Synchrotron Radiation* **2005,** *12*, 537-541.
27. Rehr, J. J.; Kas, J. J.; Vila, F. D.; Prange, M. P.; Jorissen, K., Parameter-free calculations of X-ray spectra with FEFF9. *Physical Chemistry Chemical Physics* **2010,** *12* (21), 5503-5513.
28. Perdew, J. P.; Burke, K.; Ernzerhof, M., Generalized gradient approximation made simple. *Physical Review Letters* **1996,** *77* (18), 3865-3868.
29. VandeVondele, J.; Krack, M.; Mohamed, F.; Parrinello, M.; Chassaing, T.; Hutter, J., QUICKSTEP: Fast and accurate density functional calculations using a mixed Gaussian and plane waves approach. *Computer Physics Communications* **2005,** *167* (2), 103-128.
30. Hutter, J.; Iannuzzi, M.; Schiffmann, F.; VandeVondele, J., CP2K: atomistic simulations of condensed matter systems. *Wiley Interdisciplinary Reviews-Computational Molecular Science* **2014,** *4* (1), 15-25.
31. Lin, I. C.; Seitsonen, A. P.; Tavernelli, I.; Rothlisberger, U., Structure and Dynamics of Liquid Water from ab Initio Molecular Dynamics-Comparison of BLYP, PBE, and revPBE Density Functionals with and without van der Waals Corrections. *J. Chem. Theory Comput.* **2012,** *8* (10), 3902-3910.
32. Chen, M.; Ko, H. Y.; Remsing, R. C.; Andrade, M. F. C.; Santra, B.; Sun, Z. R.; Selloni, A.; Car, R.; Klein, M. L.; Perdew, J. P.; Wu, X. F., Ab initio theory and modeling of water. *Proceedings of the National Academy of Sciences of the United States of America* **2017,** *114* (41), 10846-10851.
33. Goedecker, S.; Teter, M.; Hutter, J., Separable dual-space Gaussian pseudopotentials. *Physical Review B* **1996,** *54* (3), 1703-1710.
34. VandeVondele, J.; Hutter, J., Gaussian basis sets for accurate calculations on molecular systems in gas and condensed phases. *Journal of Chemical Physics* **2007,** *127* (11), 9.
35. Lippert, G.; Hutter, J.; Parrinello, M., A hybrid Gaussian and plane wave density functional scheme. *Molecular Physics* **1997,** *92* (3), 477-487.
36. Grimme, S.; Antony, J.; Ehrlich, S.; Krieg, H., A consistent and accurate ab initio parametrization of density functional dispersion correction (DFT-D) for the 94 elements H-Pu. *Journal of Chemical Physics* **2010,** *132* (15), 19.
37. Kepert, D. L., The Stereochemistry of Eight-co-ordination. *Journal of the Chemical Society* **1965**, 4736-4744.
38. Burdett, J. K.; Hoffmann, R.; Fay, R. C., 8-COORDINATION. *Inorg. Chem.* **1978,** *17* (9), 2553-2568.
39. Palmer, B. J.; Pfund, D. M.; Fulton, J. L., Direct modeling of EXAFS spectra from molecular dynamics simulations. *J. Phys. Chem.* **1996,** *100* (32), 13393-13398.

40. Rehr, J. J.; Kas, J. J.; Prange, M. P.; Sorini, A. P.; Takimoto, Y.; Vila, F., Ab initio theory and calculations of X-ray spectra. *C. R. Phys.* **2009,** *10* (6), 548-559.
41. Fischer, S. A.; Ueltschi, T. W.; El-Khoury, P. Z.; Mifflin, A. L.; Hess, W. P.; Wang, H. F.; Cramer, C. J.; Govind, N., Infrared and Raman Spectroscopy from Ab Initio Molecular Dynamics and Static Normal Mode Analysis: The C-H Region of DMSO as a Case Study. *Journal of Physical Chemistry B* **2016,** *120* (8), 1429-1436.
42. Valiev, M.; Bylaska, E. J.; Govind, N.; Kowalski, K.; Straatsma, T. P.; Van Dam, H. J. J.; Wang, D.; Nieplocha, J.; Apra, E.; Windus, T. L.; de Jong, W., NWChem: A comprehensive and scalable open-source solution for large scale molecular simulations. *Computer Physics Communications* **2010,** *181* (9), 1477-1489.
43. Apra, E.; Bylaska, E. J.; de Jong, W. A.; Govind, N.; Kowalski, K.; Straatsma, T. P.; Valiev, M.; van Dam, H. J. J.; Alexeev, Y.; Anchell, J.; Anisimov, V.; Aquino, F. W.; Atta-Fynn, R.; Autschbach, J.; Bauman, N. P.; Becca, J. C.; Bernholdt, D. E.; Bhaskaran-Nair, K.; Bogatko, S.; Borowski, P.; Boschen, J.; Brabec, J.; Bruner, A.; Cauet, E.; Chen, Y.; Chuev, G. N.; Cramer, C. J.; Daily, J.; Deegan, M. J. O.; Dunning, T. H.; Dupuis, M.; Dyall, K. G.; Fann, G. I.; Fischer, S. A.; Fonari, A.; Fruchtl, H.; Gagliardi, L.; Garza, J.; Gawande, N.; Ghosh, S.; Glaesemann, K.; Gotz, A. W.; Hammond, J.; Helms, V.; Hermes, E. D.; Hirao, K.; Hirata, S.; Jacquelin, M.; Jensen, L.; Johnson, B. G.; Jonsson, H.; Kendall, R. A.; Klemm, M.; Kobayashi, R.; Konkov, V.; Krishnamoorthy, S.; Krishnan, M.; Lin, Z.; Lins, R. D.; Littlefield, R. J.; Logsdail, A. J.; Lopata, K.; Ma, W.; Marenich, A. V.; del Campo, J. M.; Mejia-Rodriguez, D.; Moore, J. E.; Mullin, J. M.; Nakajima, T.; Nascimento, D. R.; Nichols, J. A.; Nichols, P. J.; Nieplocha, J.; Otero-de-la-Roza, A.; Palmer, B.; Panyala, A.; Pirojsirikul, T.; Peng, B.; Peverati, R.; Pittner, J.; Pollack, L.; Richard, R. M.; Sadayappan, P.; Schatz, G. C.; Shelton, W. A.; Silverstein, D. W.; Smith, D. M. A.; Soares, T. A.; Song, D.; Swart, M.; Taylor, H. L.; Thomas, G. S.; Tipparaju, V.; Truhlar, D. G.; Tsemekhman, K.; Van Voorhis, T.; Vazquez-Mayagoitia, A.; Verma, P.; Villa, O.; Vishnu, A.; Vogiatzis, K. D.; Wang, D.; Weare, J. H.; Williamson, M. J.; Windus, T. L.; Wolinski, K.; Wong, A. T.; Wu, Q.; Yang, C.; Yu, Q.; Zacharias, M.; Zhang, Z.; Zhao, Y.; Harrison, R. J., NWChem: Past, present, and future. *Journal of Chemical Physics* **2020,** *152* (18).
44. Metz, B.; Stoll, H.; Dolg, M., Small-core multiconfiguration-Dirac-Hartree-Fock-adjusted pseudopotentials for post-d main group elements: Application to PbH and PbO. *Journal of Chemical Physics* **2000,** *113* (7), 2563-2569.
45. Weigend, F.; Ahlrichs, R., Balanced basis sets of split valence, triple zeta valence and quadruple zeta valence quality for H to Rn: Design and assessment of accuracy. *Physical Chemistry Chemical Physics* **2005,** *7* (18), 3297-3305.
46. Adamo, C.; Barone, V., Toward reliable density functional methods without adjustable parameters: The PBE0 model. *Journal of Chemical Physics* **1999,** *110* (13), 6158-6170.
47. Grimme, S.; Antony, J.; Ehrlich, S.; Krieg, H., A consistent and accurate ab initio parametrization of density functional dispersion correction (DFT-D) for the 94 elements H-Pu. *Journal of Chemical Physics* **2010,** *132* (15).
48. Klamt, A.; Schuurmann, G., COSMO - A NEW APPROACH TO DIELECTRIC SCREENING IN SOLVENTS WITH EXPLICIT EXPRESSIONS FOR THE SCREENING ENERGY AND ITS GRADIENT. *Journal of the Chemical Society-Perkin Transactions 2* **1993,** (5), 799-805.
49. Fulton, J. L.; Bylaska, E. J.; Bogatko, S.; Balasubramanian, M.; Cauet, E.; Schenter, G. K.; Weare, J. H., Near-Quantitative Agreement of Model-Free DFT-MD Predictions with XAFS Observations of the Hydration Structure of Highly Charged Transition-Metal Ions. *Journal of Physical Chemistry Letters* **2012,** *3* (18), 2588-2593.
50. Kragten, J.; Decnopweever, L. G.; Grundler, P., MIXED HYDROXIDE COMPLEX-FORMATION AND SOLUBILITY OF BISMUTH IN NITRATE AND PERCHLORATE MEDIUM. *Talanta* **1993,** *40* (4), 485-490.
51. Tooth, B. The Hydrothermal Chemistry of Bismuth and The Liquid Bismuth Collector Model. University of Adelaide, 2013.

52. Kweon, K. E.; Hwang, G. S., Hybrid density functional study of the structural, bonding, and electronic properties of bismuth vanadate. *Physical Review B* **2012,** *86* (16).
53. Wheeler, R. A.; Kumar, P., STEREOCHEMICALLY ACTIVE OR INACTIVE LONE PAIR ELECTRONS IN SOME 6-COORDINATE, GROUP-15 HALIDES. *Journal of the American Chemical Society* **1992,** *114* (12), 4776-4784.
54. Marx, D.; Tuckerman, M. E.; Hutter, J.; Parrinello, M., The nature of the hydrated excess proton in water. *Nature* **1999,** *397* (6720), 601-604.
55. Baer, M. D.; Fulton, J. L.; Balasubramanian, M.; Schenter, G. K.; Mundy, C. J., Persistent Ion Pairing in Aqueous Hydrochloric Acid. *Journal of Physical Chemistry B* **2014,** *118* (26), 7211-7220.
56. Fulton, J. L.; Balasubramanian, M., Structure of Hydronium (H3O+)/Chloride (Cl-) Contact Ion Pairs in Aqueous Hydrochloric Acid Solution: A Zundel-like Local Configuration. *Journal of the American Chemical Society* **2010,** *132* (36), 12597-12604.
57. Baer, M. D.; Pham, V. T.; Fulton, J. L.; Schenter, G. K.; Balasubramanian, M.; Mundy, C. J., Is Iodate a Strongly Hydrated Cation? *Journal of Physical Chemistry Letters* **2011,** *2* (20), 2650-2654.

Table of Contents artwork

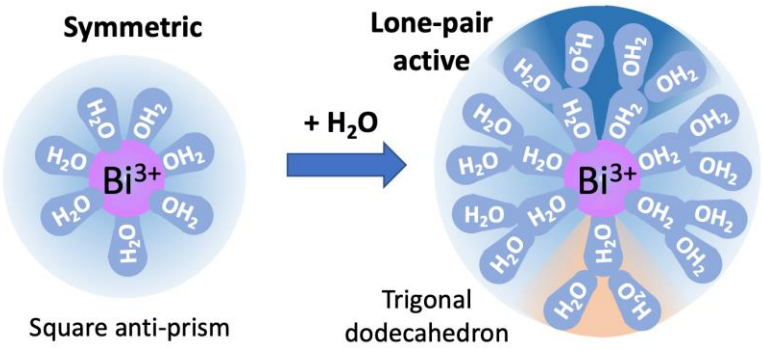

Synopsis

Water hydrating aqueous Bi^{3+} is highly ordered in an arrangement controlled by the 6*s*2 active lone-pair configuration. Furthermore, water provides a non-centrosymmetric solvent environment through a non-uniformity between the first- to second-shell H-bonding arrangement that stabilizes the Bi^{3+} lone-pair electronic state. DFT-MD simulations and hybrid DFT methods provide crucial insights into these structures that can be compared directly to experimental EXAFS.